DOI: https://doi.org/10.53350/pjmhs22169862

ORIGINAL ARTICLE

The Subline of Metastatic Prostate Cancer Cell line, DU145 expresses Tks4 and reveals distinctive Phenotype

ALDHAFEERI HQ[1], LEONG HS[2]
[1]*Department of Medical Laboratory, College of Applied Medical Sciences, Majmaah University, Majmaah, Saudi Arabia*
[2]*Sunnybrook Health Sciences Centre, Toronto, ON, Canada*
Correspondence to: Aldhafeeri Hq

ABSTRACT

Cancer metastasis is the process of dissemination of cancer cells from their original site and localization in distant sites. During this journey, metastatic cancer cells have to undergo several phenotypical/ genotypical changes for acquiring cell migration, invasion, attachment properties etc. These steps can be partially/fully mimicked under in vivo and in vitro conditions. Here, we injected metastatic prostate cancer cell line, DU145, into the chorioallantoic membrane (CAM) of the chicken embryo to generate sublines which were isolated 7-days post-injection, and subcultured under in vitro conditions. Our results showed that one of these sublines, DC-1-, exhibited a distinctive phenotype compared with the parental cell line when grown in 3D culture model. Further, the expression of Tks4 at the mRNA and protein level in DC-1- cells was observed to be higher than the regular DU145 cells.

Keywords: Prostate cancer, DU145, DC-1-, Metastasis, Round, Stellate, Colony, Tks4

INTRODUCTION

Prostate cancer (PCa) is the most diagnosed disease in the developed world. It is more likely to affect elderly people compared to other age groups [1]. There are multiple factors that contribute to PCa formation, such as nutrition factors, habit-related factors, androgens, and ethnicity [1]. The Multiethnic Cohort Study (MCS) for statistics revealed that PCa is largely diagnosed in men of African descent compared to their ethnic counterparts in the United States [2,3]. Patients with prostate cancer are treated with hormone therapy called androgen deprivation therapy (ADT). ADT inhibits androgen production from its main source or blocks its cellular receptor-mediating signaling cascade [1]. In addition, blocking critical pathways for PCa such as Hedgehog, fibroblast growth factor (FGF), transforming growth factor beta (TGF-β), Src, and integrins has been used for PCa patients [4]. Some patients cease to respond to this therapy and develop resistance. This resistance allows PCa to progress in an androgen-independent manner. The second line of treatment is chemotherapy, which is typically docetaxel and cabazitaxel. These treatments stabilize microtubules of rapidly dividing cells [5] and can extend the survival rate by 2-4 months [6,7]. Other drugs can be used as a second line treatment are based on the individual patient characteristics such as sipuleucel-T (immunotherapy) and radium-233 dichloride (^{223}R) (radiotherapy) [8,9]. Resistance to ADT is also associated with migration of PCa to distant sites such as the bone, brain, liver, and lymph nodes, by a process called metastasis.

Cancer metastasis is the leading cause of cancer related-death [10]. Metastasis consists of four key steps: 1) intravasation, when a cancer cell detaches from the primary tumor and enters into the blood circulation, 2) extravasation, when cancer cells exit the blood circulation; 3) micrometastases formation in the new environment, and 4) colonization, when these micrometastases progress into a macroscopic tumor [11,12]. To initiate this cascade, the cancer cells must first acquire invasive characteristics [13]. One key process in acquiring an invasion capacity is the degradation of the surrounding extracellular matrix and cell protrusion formation [10]. This morphological change is followed by a phenotypic switch in cancer cells from an epithelial to mesenchymal transition (EMT). This mechanism converts the epithelial cells from its polar state into to migrating, fibroblast-like mesenchymal cells. Under physiological conditions, EMT phenomenon is a reversible process as shown during embryogenesis [14].

Cancer metastasis, overall, is an inefficient process. Very few cancer cells eventually are able to establish new metastatic colonies [15]. Therefore, metastatic cells which have intravasated into the blood circulation may not successfully go through the extravasation step, which leads to failure in extravasated cell colony formation. In addition, a significant number of extravasated cells are believed to undergo programmed death within 24 hours [16]. The surviving extravasated cells are also not guaranteed to proliferate into a cancer colony and may remain in the dormant state [17,18], [19]. Therefore, successful metastatic growth requires cancer cells to overcome a number of obstacles, such as the immune system, blood forces, a harsh environment, hypoxia, and acidity [5]. Metastatic cancer cells evade host immunity via several mechanisms. It has been reported that metastatic cells disguise themselves from natural killer cells (NK) by expressing coagulation factors VIIa and X [20,21]. Interestingly, treatment with anticoagulants has been shown to attenuate metastatic burden in animal models and in cancer patients [22].

The majority of patients (approximately 90%) with metastatic PCa develop metastases in the bone and the rest develop metastases mainly in the brain and lymph nodes. Mortality for prostate cancer metastasis is the highest compared to other bone metastasis associated cancers [6]. Patients with metastatic PCa in the bone exhibit sclerotic bone lesions associated with an increase in osteoblasts [8]. These symptoms can be mitigated at this stage by radiotherapy or osteocyte inhibitors [9]. However, cancer becomes hard to treat when it has metastasized to the bone by affecting bone remodeling processes and leaving patients with severe pain, pathological fractures, hypercalcemia, and spinal and nerve compression [23,24].

Animal models are the gold-standard for preclinical studies, especially for cancer research [25]. However, animal models are expensive and time-consuming with respect to regulatory guidelines as well as disease recapitulation. Moreover, with the exception of the genetic murine model, there is a lack of a model which mimics all metastatic cascades, including extravasation, intravasation, and colonization [26]. The avian model is an excellent option to circumvent some of these difficulties. The CAM of the chick embryo is a very thin organ composed of three layers: ectoderm, mesoderm, and endoderm [27]. The CAM functions as a respiratory system for the chick embryo since it is aligned through the porous eggshell. It enables the embryo to exchange gases through these pores, and helps transport electrolytes from allantoic sacs and calcium from the shell.

This model is naturally immunodeficient in early stages, cost-effective, amenable to real-time intravital imaging, and highly vascularized with good lymphatic drainage [25,28]. With the advancement of imaging technology, the CAM model allows tracking injected dyes and cells to illuminate the capillary network, and both extravasated and intravasated cells [15]. As mentioned earlier, the main mediator of cancer cell metastasis is the blood canal [12]. Two out of three key steps of the metastatic cascade take place in the blood vessels. Therefore, the CAM model can be used as a window for monitoring the cancer metastasis cascade. For example, we can assess micrometastases formation, extravasation efficiency, cancer cell survival, and dormancy. In addition,

intravasation efficiency can be performed via bolus injection, which takes place by injecting cells in the stroma of the CAM [27]. On-planting a Patient Derived Xenograft (PDX) on top of the CAM after slightly tearing it allows for assessment of angiogenesis..

There are limitations associated with this CAM model. Timing of this experiment is relatively short, which means macrometastases cannot be observed [29]. The survival rate for chicks after the experiment is low at 65-70% even under ideal experimental conditions. Dynamic angiogenesic responses are also difficult to observe [30]. Lastly, shell traces left following cracking of the eggs may induce inflammation and angiogenesis [30].

In my studies, we performed an intravenous injection of cells to assess tumor colony formation. In these studies, cells intravasate the blood vessels at day 9. It has been shown that there is a substantial increase in endothelial cell number at this age [25] (**Fig 1**)

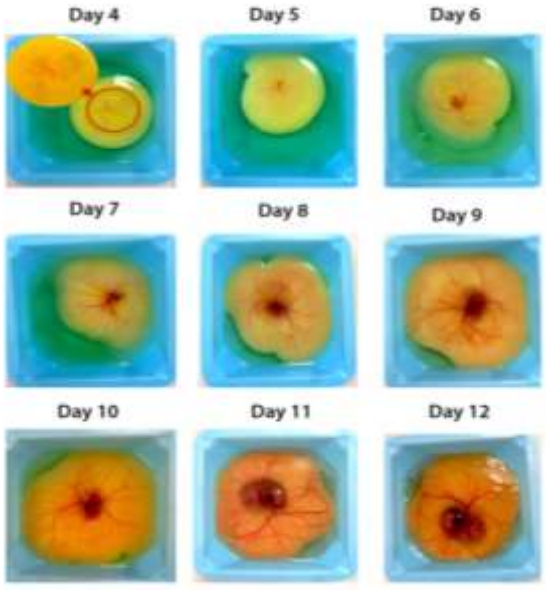

Figure **1**: Chorioallantoic Membrane (CAM) of the Chick Embryo Model after Cracking.

Fertilized eggs cracked three days after incubation were placed in a blue container. At day 9, an expansion of blood vessels seems to appear for performing an IV injection and other assays.

MATERIALS AND METHODS

Cell Culture (2D): DU145 cells are metastatic PCa cells derived from the brain [31]. These cells were maintained in DMEM. PC3-M-LN4 was initially derived from the bone [32] and was maintained in RPMI media. BPH cells, an inflammatory cell line extracted from a 68-yr-old patient undergoing transurethral resection of the prostate for urinary obstruction [33], were maintained in RPMI. All media were supplemented with 10% FBS, 100 IU/mL Penicillin, 100 µg/mL streptomycin and incubated at 37°C and 5% CO_2. DU145 and PC3-M-LN4 cell lines were lentivirally infected with a ZsGreen vector to intravitally visualize the cells in the CAM model.

Cell Culture (3D): Cells were embedded between two layers of Matrigel. For the bottom layer, 175 µL of 100% Matrigel was added into one well of the 24 well/plate and incubated at 37°C (5% CO_2) for 30 minutes to be polymerized. Cells were next counted and seeded at 1×10^4 cells/mL density (~1500 cells/ well) on top of the Matrigel layer. Cells were left for 30 minutes to allow attachment. For the upper layer, 150 µL of 20% Matrigel/culture medium was added to cover the cells. Fresh medium was added every two days. After 7-10 days, colonies were counted using the inverted microscope and/or used for cytochemistry.

CAM Injection: DU145-zsGreen and PC3-M-LN4-zsGreen cells were counted using the hemocytometer chamber and injected at 1×10^6 cells/mL density (~1×10^5 cells/CAM). The cell suspension was kept on ice prior to and during the injection period to maintain cell viability. Afterwards, the cells were injected under a dissecting microscope via a microinjector which consists of four parts: a syringe, a needle, tubing, and micropipette-pulled needle. During and after the injection, the CAM model was immediately visualized under the fluorescent microscope to confirm cell injection. After 7 days, micrometastases were either counted for colony formation efficiency or extracted for passaging and injection.

Extracting micrometastases out of the CAM: After 7 days post injection into the CAM and under the fluorescent microscope, colonies of interest were picked up by fine forceps and cut out by fine scissors. Then, the extracted colonies were individually dissected from any associated extra tissue by a sterile scalpel. Each colony was sub-cultured in one well of the 24 well/plate and fed with the preferred medium supplemented with (10X) hyaluronidase, (10X) collagenase, and a potent antibiotic (100X) normocin.

DNA Extraction from Mammalian Cells: Total DNA was purified from the transduced cells using Puregene Core Kit A (Qiagen) following the manufacturer's instructions. Three hundred µL of cell lysis solution was added to the cell pellet and vigorously agitated at high speed for 10 seconds. Ten µL of protein precipitation solution was added and vigorously agitated at high speed for 20 seconds. Subsequent centrifugation for the mixture was performed for 1 minute at 16,000 x g. The supernatant was gently poured out into 300 µL of isopropanol in a centrifuge tube. The mixture solution was manually and gently inverted 50 times. Subsequent centrifugation was performed for 1 minute at 16,000 x g, and the supernatant was discarded leaving behind a white DNA pellet. The DNA pellet was washed with 300 µL of 70% ethanol and spun down for 1 minute at 16,000 x g. The supernatant was discarded, and the DNA pellet was left to air dry for 5 minutes. One hundred µL DNA hydration solution was added and incubated at 65°C for 1 hour to dissolve the DNA. DNA was quantified using the NanoDrop™ 1000 Spectrophotometer (Thermo Fisher Scientific). DNA samples were then amplified using standard PCR for sequencing.

Table 1: List of PCR primers

Gene	Sequence
Tks4	F: GCGTCGAGACCCAACTTTCT R: TCTTTAGACCATGGCAACCCC
β-Actin	F: AGAGCTACGAGCTGCCTGAC R: AGCACTGTGTTGGCGTACAG

Immunofluorescence (2D): Eight mm glass coverslips were placed in 24 well/plate prior to cell culture. The cells were grown on top of these coverslips overnight. Cells were then fixed using 10% formalin for 15 minutes. Cells were washed three times and then blocked and permeabilized by a mixture of 0.01% Triton™ X-100 and 1% BSA. Primary antibody was diluted in 1% BSA at appropriate dilution (1:1000) and incubated at 4°C overnight. The primary antibody solution was aspirated, and the coverslips were then washed three times with PBS. The secondary antibody was diluted in 1% BSA at appropriate dilution (1:2000) and incubated at room temperature for an hour. Prolong mounting medium with DAPI (Invitrogen Cat. P36931), was dropped on top of the slides, and the coverslips were placed upside down on the slide. The cells were then visualized under the confocal microscope. A list of antibodies used is given in **Table 2**.

Immunofluorescence (3D): Small dishes with glass at the bottom (MatTek Cat. No. P35G-0-10-C) were used to enhance imaging resolution for this assay. Prior to staining, cells were immersed in Matrigel (Corning® Cat. No. CACB354234) as previously demonstrated in Section (2.2). Cells were fixed by adding a

mixture of 20% acetone and 80% methanol and incubated for 20 minutes at 4°C. After aspirating the fixative, cells were gently washed 3X with PBS to protect the Matrigel, and 3% BSA was subsequently used for blocking for 1 hour. Primary antibody was diluted in 3% BSA at low dilution (1:200) and incubated for one hour. Secondary antibody, diluted as above, was added for one hour. Prolong mounting medium with DAPI was gently dropped on top of cell matrix and a square cover slip was placed on top of it. The colonies were then visualized under the confocal microscope.

Table 2: List of Fluorescent Dyes and Antibodies

Fluorescent Materials	Source (Cat. Number)
Anti-human Tks4 Antibody	Milliporesigma (09-267)
Anti-β-Actin Antibody	abm (G043)
Alexa Fluor™ 488 Phalloidin	ThermoFisher (A22287)
ProLong™ Gold Antifade Mountant with DAPI	ThermoFisher (P36931)
Dextran	ThermoFisher (D1868)
DyLight 649 labeled Lens Culinaris Agglutinin (LCA) (Lectin)	Vector Laboratories (DL-1048)

qRT-PCR: Total RNA was isolated from cells using RNAeasy Mini kit (Qiagen). In brief, the cells were lysed with 300 µL of cell lysis buffer and subsequently agitated at high speed and centrifuged for 3 minutes at maximum speed. The supernatant was gently aspirated and mixed with 300 µL of 70% ethanol. The total volume was then transferred onto RNeasy Mini spin column in a 2-mL collection tube and centrifuged for 15 s at ≥8000 x g. The flow-through was discarded. The spin column was washed with 700 µL of washing buffer and centrifuged for 3 minutes. The column was then placed in a new centrifuge tube, and 30 µL of RNase-free water was added and centrifuged for 2 minutes. RNA was quantified using the NanoDrop™ 1000 Spectrophotometer (Thermo Fisher Scientific). One µg of RNA was reverse transcribed to cDNA using qScript™ cDNA Synthesis Kit (QuantaBiosciences). One hundred ng of cDNA was amplified with primers listed in Table 1. Actin was used as the housekeeping gene. Samples were run on QuantStudio 5 qPCR (Thermofischer Scientific US). For each reaction, 1 µL of 10 µM forward/reverse primers, 1 µL of 100 ng DNA template, 5 µL SYBR Green qPCR Mastermix, and Nuclease-free water was added to yield a 10 µL reaction mixture. The PCR conditions were 40 cycles of denaturation at 95°C for 15s and annealing at 60°C for 1 min followed by a melt curve stage.

Western blotting: Lysate mixture consisting of RIPA buffer (Sigma-Aldrich Cat. No. R0278-50ML) and protease inhibitor cocktail was added to the cells, and cells were lysed using a cell scraper. Proteins from different cell lines were then quantified by the Bradford assay. Ten-times Reducing agent and 4X sodium dodecyl sulfate (SDS) were added based on protein quantity. Samples were then boiled for 10 minutes for protein denaturation. Samples were run on a gel at 120 V for an hour. Polyvinylidene difluoride (PVDF) membrane was immersed in methanol to be activated and placed within sponges, filter papers as well as the gel and transferred at 30 V for 2 hours. PVDF membrane was then blocked with 1-3% skim milk in TBS-T and incubated in 1 hour at RT. Primary antibody was diluted at appropriate concentration (1:1000) in 1-3% skim milk/TBS-T and added to the membrane and incubated overnight at 4°C. The membrane was then washed three times with TBS-T for 15 minutes, and secondary antibody was subsequently added after being diluted in 1-3% skim milk/TBS-T (1:5000) and incubated in an hour at RT. One mL of Luminata Crescendo Western HRP substrate (Millipore_Sigma Cat. WBLUR0100) was added on top of the PVDF membrane, and protein bands were developed and visualized using the ChemiDoc XRS System.

Confocal microscopy: Intravital and confocal images were captured using a Nikon Fast A1R Resonance Confocal Microscope as described previously [34]. To capture circulating cancer cells and/or established colonies in the CAM, Lectin (binds to glycocalyx on the endothelial cells) and Dextran dyes were injected into the CAM to illuminate the vessel lumen and the luminal surface of endothelial cells. The model was then placed in a special chamber with a special lid with a centered hole for placing coverslip to maintain position.

Statistical Analysis: GraphPad prism software was used for all tests. A one-tailed unpaired student t-test was used for analysis. Data are presented as mean ± standard deviation (SD). A probability value $P < 0.05$ was considered statistically significant.

RESULTS

DU145 PCa cells are more effective at metastatic formation exhibiting a higher percentage of stellate morphology: There are many metastatic PCa lines and it is not clear which are more metastatic or aggressive [15,35]. Thus, two metastatic PCa cell lines were evaluated in vivo for their morphology and ability to form metastases. DU145 cells and PC-3M-LN4 cells were injected at 1×10^6 cells/mL (~1×10^5 cells/CAM) into embryonic Day 9 chicken embryos. These cells were permanently expressing ZsGreen by viral transduction for visualization under fluorescence stereoscopy. At 7-days post-injection, we counted the number of cancer colonies using fluorescence stereoscopy and enumerated stellate-shaped colonies versus non-stellate colonies. In an in vivo model, metastatic cells usually form more stellate colonies in the CAM model compared to round colonies seven days post-injection. Our results showed that DU145 PCa cell line is more effective at metastatic colony formation and that the majority of these exhibit a stellate morphology (**Fig *2***)

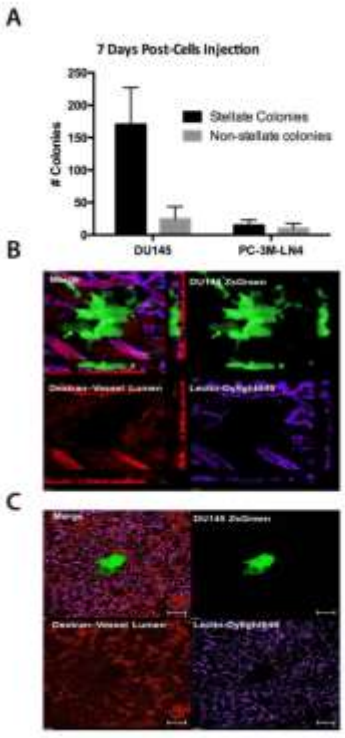

Figure **2**: DU145 cells exhibited higher metastatic efficiency and a higher percentage of stellate morphology relative to PC-3M-LN4 cells

A A bar graph showing that DU145 cells form more colonies (170.1 ± 13.5 colonies/embryo) than the PC-3M-LN4 cells (24.4 ± 4.5). Ninety percent of DU145 colonies exhibited a stellate morphology compared to only 35% for PC-3M-LN4. **B**) Representative image for a DU145 stellate colony established in the CAM stroma at 7-days post-injection. **C**) Representative image for a DU145 round colony established in the CAM stroma at 7-days

post-injection, Lectin and Dextran dyes were used to illuminate blood vessels. Results as a mean +/- SD.

Isolation of stellate colonies from the CAM model and subculture: We then sought to establish a cell line with new characteristics. It has been shown that serially culturing metastatic colonies after isolation from the host will enrich the isolated cells with more aggressive characteristics relative to the parental cells. Thus, we isolated a total of 70 CAM-colonies from DU145 that exhibit a stellate phenotype and passaged them in culture **(Fig *3*)**.

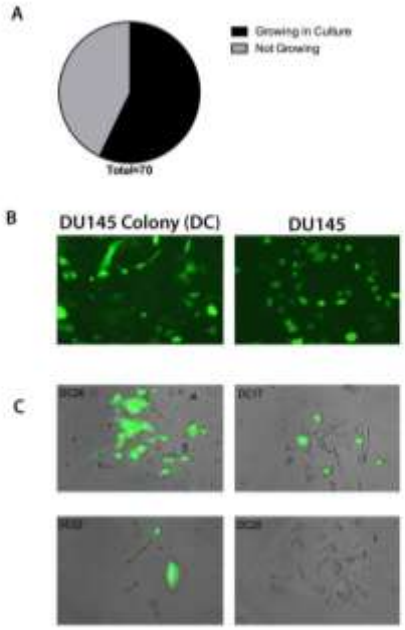

Figure **3**: Isolation of stellate colonies from the CAM model and subculture

A A pie chart demonstrating 40 of the isolated colonies that grew in culture. **B**) A simple comparison in 2D culture between regular DU145 and an isolated colony. **C**) Representative images of isolated colonies growing in culture using the bright field with the green channel. DC#: DU145 Colony#.

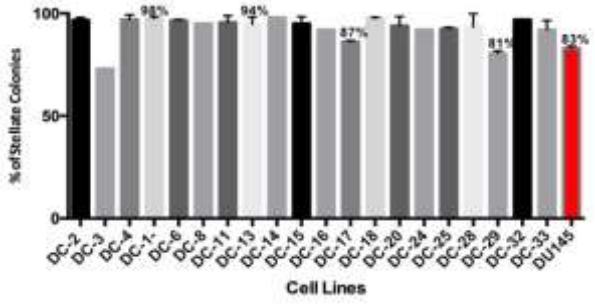

Figure **4**: DU145 sublines formed higher percentage of stellate colonies compared to the parental cells

DU145 sublines increased the percentage of stellate colonies: Only 40 out of 70 isolated colonies were able to grow in culture. Colonies failed to grow in culture mostly due to technical errors. Other growing colonies grew in culture but divided at a low rate or were contaminated. These were all discarded. A total of 20 colonies were contamination-free and grew in culture. These were injected into the CAM model in order to evaluate whether their stellate phenotype is enhanced. The number of stellate colonies were counted at 7-days post-injection **(Fig *4*)**.

A bar graph showing that the second round cancer cell formed relatively higher percentage of stellate colonies (93-98%) compared to parental DU145 (83%) (shown in red) after one round of in vivo passaging. Results as a mean +/- SD. DC#: DU145 Colony#.

DC-1- subline formed invadopodia and expressed Tks4: All sublines, after being injected into the CAM model, produced colonies that have relatively similar stellate morphology compared to the original cell line DU145, except DC-1- subline which produced a distinctive phenotype in its stellate form.

In order to evaluate further, we plated DU145 and DC-1- in Matrigel. This assay closely mimics the in vivo environment by allowing the cells to expand clonally in a 3D environment surrounded by matrix. After 7 days, both cell lines form colonies with a mixture of stellate and round morphology. Interestingly, DC-1- cells formed protrusions mimicking invadopodia (**Fig 5A-B**). These protrusions were not seen in DU145 cells.

We next examined these cell lines at the molecular level. A body of evidence revealed that Tks4 is responsible for protrusion formation, especially invadopodia [36]. Our results showed that DC-1- robustly express Tks4 at the mRNA and protein level over the regular DU145 (**Fig 5C-D**).

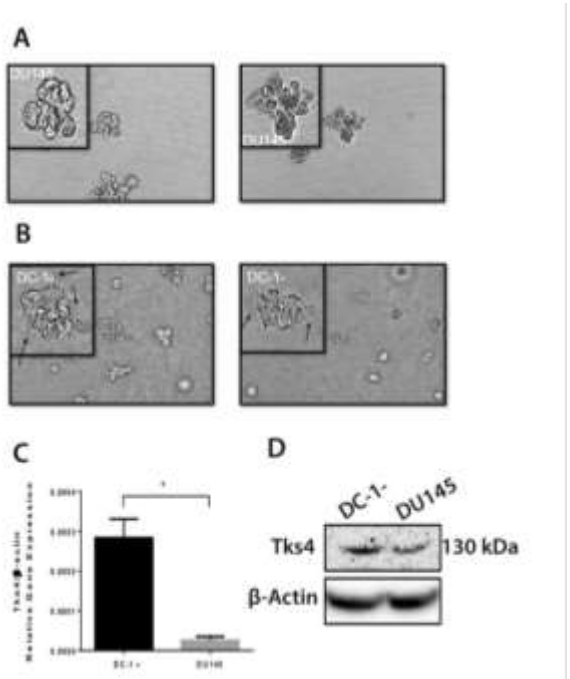

Figure **5**: DC-1- subline form invadopodia and express Tks4

A Two representative images of DU145 colony in stellate state that did not form any protrusions when plated in 3D culture model (insets show higher magnification images). **B**) DC-1- forming protrusions (insets show higher magnification images). Black arrows indicating protrusions. **C**) qPCR analysis of Tks4 mRNA revealing that DC-1- expressed Tks4. **D**) Immunoblotting showing high expression of Tks4 in DC-1- subline relative to the original DU145. β-actin was used as a loading control and a housekeeping gene. $^{*}p<0.05$.

DISCUSSION

This avian model is convenient, cost-effective, highly vascularized (**Fig 1**), and amenable to real-time imaging. We injected metastatic PCa cell lines into the CAM model to monitor the morphology of colonies at 7-days post-injection. These colonies were expected to

produce a homogenous “stellate” morphology [37] indicating an aggressive cell behaviour.

The CAM injection results for both cell lines revealed compatible results with previous work regarding metastasis [38]. Metastasis is an inefficient process, and this has been extensively studied. Luzzi and colleagues have shown that only 0.02% of the melanoma B16F10 cells form metastases in the animal model [39]. The metastatic efficiency for PC-3M-LN4 was found to be 0.03%, and 0.1% for DU145 in the CAM model. Surprisingly, the results for comparing the metastatic potential between both cell lines after injection into the CAM showed that the DU145 cells were three times more likely to be metastatic compared to the PC-3M-LN4 cell line (**Fig 2**). There are three classical PCa cell lines: PC-3M-LN4, DU145, and LNCaP. The two former cell lines are androgen-independent, and the later one is androgen-dependent [40]. Our group showed that these androgen-independent cells are highly metastatic compared to LNCaP [data not shown]. PC-3M-LN4 is a highly representative of PCa metastatic ability [41,42], [43] relative to DU145 [44]. Furthermore, it is a subline of PC-3 which is a metastatic PCa cell line derived from the human bone. PC-3 was injected and metastasized to the lymph node of the mice. This cycle has been rounded four times [32]. This number of passages of the cell line is expected to make it more aggressive and metastatic than DU145 cell line. Two explanations may be formulated from these observations. First is the extravasation step at day 9 for the CAM injection. The results from the extravasation assay, which typically starts at day 13 of the chicken embryo, revealed that PC-3M-LN4 extravasates well when compared with day 9 injection (0.03% vs 0.09%) [data not shown]. Injection at day 9 for the colony formation assay is of a critical importance because the lifetime for the embryos is limited to 18-20 days [28]. Thus, injection of cells at the early age will allow them to proliferate into a colony. Second, the DU145 cell line may have higher metastatic potential since this line is derived from the brain and would have penetrated the blood-brain barrier (BBB) [45,46]. Metastatic cancer cells tend to metastasize to the brain at a very late stage compared with other distant sites [47]. Another study showed that DU145 can proliferate in the bone environment after intratibial inoculation into the mouse [48], whereas the LNCaP cell line did not survive or proliferate [49,50]. These studies suggest that the DU145 cell line may be similar to PC-3, which is a bone-derived cell line.

Multiple lines of evidence have shown that a subline may have distinctive differences from the parental population in melanoma [51], breast cancer [52,53], and prostate cancer [32]. Serial passages of PCa cells could potentiate the cells' metastatic potential by facilitating genetic alterations and independence from androgen hormones [32]. Therefore, we sought to do the same and isolate a subline with more invasive properties (**Fig 3**), which eventually will form a different morphology compared to the parental cell line. Overall, most of the generated sublines showed a high degree of invasiveness by forming a greater percentage of stellate colonies relative to the parental DU145 cells after injection into the CAM model (**Fig 4**).

Interestingly, DC-1- subline showed distinctive properties over the original DU145 cell line. DC-1- formed protrusions after plating in 3D culture Matrigel and significantly expressed Tyrosine kinase substrate with four SH3 domains-4 (Tks4) at mRNA as well as at the protein level (**Fig 5**). Tks4 is an adapter protein that is well known for protrusion formation, podosome formation and cell adhesion [36]. The status of a related protein, Tks5, in DU145 is unknown. We evaluated the mRNA levels of Tks5 in both cell lines, and neither showed any positivity. This might due to the environment for the cells during harvesting prior RNA extraction. Tks5 is a very well known mediator for invadopodia formation, a critical protrusive structure for facilitating cell extravasation [54]. We also speculate that these are not lamellipodia, because this lamellipodia protrusion appears only in 2D culture [55,56]. Invadopodia and lamellipodia are hard to distinguish [54,57]. Podosomes are distinctive from invadopodia since the former are found in normal cells such as macrophages and endothelial cells, and invadopodia are found in neoplastic cells [58]. However, they share strong similarities that they are both included under the umbrella term invadosome [59]. Other markers can be used to identify protrusion formation, in particular invadopodia, including cortactin and the neural Wiskott-Aldrich Syndrome protein (N-WASP).

There is a need to further test Tks4 function in PCa using the three classical PCa cell lines: PC-3, DU145, and LNCaP. Evaluating its expression at the protein and mRNA levels would be useful for determining if these cells have an altered function of this gene product. Knocking this gene out/in could be used to evaluate its contribution to colony formation or morphological changes in 3D culture. Forming colonies in soft agar has been correlated with tumorigenesis[60]. Performing cell migration and cell invasion assays would help to determine whether silencing this gene would attenuate or potentiate tumorigenesis in these cell lines.

Acknowledgment: This research was partially supported by The Ministry of Education in Saudi Arabia.

Conflicts of Interest: The authors declare no conflict of interest

REFERENCES

1. Nelson WG, De Marzo AM, Isaacs WB, Wgn P, Wgn U. Prostate Cancer. n engl j med. 2003;3494349:366-381.
2. Henderson BE, Lee NH, Seewaldt V, Shen H. The influence of race and ethnicity on the biology of cancer. Nat Rev Cancer. 2012;12(9):648-653. doi:10.1038/nrc3341
3. Kolonel LN, Altshuler D, Henderson BE. The multiethnic cohort study: exploring genes, lifestyle and cancer risk. Nat Rev Cancer. 2004;4(7):519-527. doi:10.1038/nrc1389
4. Karlou M, Tzelepi V, Efstathiou E. Therapeutic targeting of the prostate cancer microenvironment. Nat Rev Urol. 2010;7(9):494-509. doi:10.1038/nrurol.2010.134
5. Steeg PS, Ouatas T, Halverson D, Palmieri D, Salerno M. Metastasis suppressor genes: Basic biology and potential clinical use. Clin Breast Cancer. 2003;4(1):51-62. doi:10.3816/CBC.2003.n.012
6. Parker C, Nilsson S, Heinrich D, et al. Alpha Emitter Radium-223 and Survival in Metastatic Prostate Cancer. N Engl J Med. 2013;369(3):213-223. doi:10.1056/NEJMoa1213755
7. De Bono JS, Oudard S, Ozguroglu M, et al. Prednisone plus cabazitaxel or mitoxantrone for metastatic castration-resistant prostate cancer progressing after docetaxel treatment: A randomised open-label trial. Lancet. 2010;376(9747):1147-1154. doi:10.1016/S0140-6736(10)61389-X
8. Makhoul I, Montgomery CO, Gaddy D, Suva LJ. The best of both worlds — managing the cancer, saving the bone. Nat Rev Endocrinol. 2015;12(1):29-42. doi:10.1038/nrendo.2015.185
9. Body J-J, Casimiro S, Costa L. Targeting bone metastases in prostate cancer: improving clinical outcome. Nat Rev Urol. 2015;12(6):340-356. doi:10.1038/nrurol.2015.90
10. Chaffer CL, Weinberg R. A Perspective on Cancer Cell Metastasis. Science (80-). 2011;331(6024):1559-1564. doi:10.1126/science.1203543
11. Hanahan D, Weinberg RA. Hallmarks of cancer: The next generation. Cell. 2011;144(5):646-674. doi:10.1016/j.cell.2011.02.013
12. Chambers AF, Groom Ac Fau - MacDonald IC, MacDonald IC, Nat Rev C. Dissemination and growth of cancer cells in metastatic sites. Nat Rev Cancer. 2002.
13. Weber GF. Why does cancer therapy lack effective anti-metastasis drugs? Cancer Lett. 2013;328(2):207-211. doi:10.1016/j.canlet.2012.09.025
14. Bacac M, Stamenkovic I. Metastatic cancer cell. Annu Rev pathmechdis Mech Dis. 2008. doi:10.1146/annurev.pathmechdis.3.121806.151523
15. Kim Y, Williams KC, Gavin CT, Jardine E, Chambers AF, Leong HS. Quantification of cancer cell extravasation in vivo. 2016;11(5). doi:10.1038/nprot.2016.050
16. Sahai E. Illuminating the metastatic process. Nat Rev Cancer. 2007;7(10):737-749. doi:10.1038/nrc2229
17. Naumov GN, Macdonald IC, Weinmeister PM, et al. Persistence of Solitary Mammary Carcinoma Cells in a Secondary Site : A Possible Contributor to Dormancy Persistence of Solitary Mammary Carcinoma Cells in a Secondary Site : A Possible Contributor to Dormancy 1. 2002:2162-2168.
18. Goss PE, Chambers AF. Does tumour dormancy offer a therapeutic target? Nat Publ Gr. 2010;10(12):871-877. doi:10.1038/nrc2933
19. Holmgren L, O'Reilly MS, Folkman J. Dormancy of micrometastases: balanced proliferation and apoptosis in the presence of angiogenesis

suppression. Nat Med. 1995;1:149-153. doi:10.1038/nm0295-149
20. Im JH, Fu W, Wang H, et al. Coagulation Facilitates Tumor Cell Spreading in the Pulmonary Vasculature during Early Metastatic Colony Formation Coagulation Facilitates Tumor Cell Spreading in the Pulmonary Vasculature during Early Metastatic Colony Formation. 2004:8613-8619. doi:10.1158/0008-5472.CAN-04-2078
21. Palumbo JS. Mechanisms Linking Tumor Cell – Associated Procoagulant Function to Tumor Dissemination. 2008;1(212):154-160. doi:10.1055/s-2008-1079255.
22. Nash GF, Turner LF, Scully MF, Kakkar AK. Platelets and cancer. Lancet Oncol. 2002;3(7):425-430. doi:10.1016/S1470-2045(02)00789-1
23. Weilbaecher KN, Guise TA, McCauley LK. Cancer to bone: a fatal attraction. Nat Rev Cancer. 2011;11(6):411-425. doi:10.1038/nrc3055
24. Roodman GD. Mechanisms of Bone Metastasis. N Engl J Med. 2004;350(16):1655-1664. doi:10.1056/NEJMra030831
25. Segura PNT, Iruela-arispe ML. The chicken chorioallantoic membrane model in biology , medicine and bioengineering. 2014:779-804. doi:10.1007/s10456-014-9440-7
26. Faltermeier CM, Drake JM, Clark PM, Smith BA, Zong Y, Volpe C. Functional screen identifies kinases driving prostate cancer visceral and bone metastasis. 2015. doi:10.1073/pnas.1521674112
27. Deryugina EI, Quigley JP. Chick embryo chorioallantoic membrane model systems to study and visualize human tumor cell metastasis. 2008:1119-1130. doi:10.1007/s00418-008-0536-2
28. Cimpean AM, Ribatti D, Raica M. The chick embryo chorioallantoic membrane as a model to study tumor metastasis. Angiogenesis. 2008;11(4):311-319. doi:10.1007/s10456-008-9117-1
29. Chambers AF, Shafir R, Ling V. A Model System for Studying Metastasis Using the Embryonic Chick1. 1982;42(October):4018-4025.
30. Staton CA, Reed MWR, Brown NJ. A critical analysis of current in vitro and in vivo angiogenesis assays. Int J Exp Pathol. 2009;90(3):195-221. doi:10.1111/j.1365-2613.2008.00633.x
31. Stone KR, Mickey DD, Wunderli H, Mickey GH, Paulson DF. Isolation of. 1978;281:274-281.
32. Pettaway CA, Pathak S, Greene G, et al. Selection of Highly Metastatic Variants of Different Human Prostatic Carcinomas Using Orthotopic Implantation in Nude Mice. Clin Cancer Res. 1996. doi:10.1361/foec2000p001
33. Hayward SW, Dahiya R, Cunha GR, Bartek J, Deshpande N, Narayan P. Establishment and characterization of an immortalized but non-transformed human prostate epithelial cell line: BPH-1. Vitr Cell Dev Biol - Anim. 1995;31(1):14-24. doi:10.1007/BF02631333
34. Leong HS, Steinmetz NF, Ablack A, et al. Intravital imaging of embryonic and tumor neovasculature using viral nanoparticles. Nat Protoc. 2010;5(8):1406-1417. doi:10.1038/nprot2010-103
35. Orr FW, Lee J, Duivenvoorden WC, Singh G. Pathophysiologic interactions in skeletal metastasis. Cancer. 2000;88(12 Suppl):2912-2918. doi:10.1002/1097-0142(20000615)88:12+<2912::AID-CNCR6>3.0.CO;2-8
36. Buschman MD, Bromann PA, Cejudo-martin P, Wen F, Pass I, Courtneidge SA. The Novel Adaptor Protein Tks4 (SH3PXD2B) Is Required for Functional Podosome Formation. Mol Biol Cell. 2009. doi:10.1091/mbc.E08
37. Lyons SM, Alizadeh E, Mannheimer J, et al. Changes in cell shape are correlated with metastatic potential in murine and human osteosarcomas. Biol Open. 2016;5(3):289-299. doi:10.1242/bio.013409
38. Fidler IJ. Metastasis: quantitative analysis of distribution and fate of tumour emboli labeled with 125I-5-iodo-2[prime]-deoxyuridine. J Natl Cancer Inst. 1970;45:773-782.
39. Luzzi KJ, MacDonald IC, Schmidt EE, et al. Multistep Nature of Metastatic Inefficiency. Am J Pathol. 1998;153(3):865-873. doi:10.1016/S0002-9440(10)65628-3
40. Minamiguchi K, Kawada M, Someno T, Ishizuka M. Androgen-independent prostate cancer DU145 cells suppress androgen-dependent growth of prostate stromal cells through production of inhibitory factors for androgen responsiveness. Biochem Biophys Res Commun. 2003;306(3):629-636. doi:10.1016/S0006-291X(03)01023-4
41. Zvieriev V, Wang JC, Chevrette M. Over-expression of CD9 does not affect in vivo tumorigenic or metastatic properties of human prostate cancer cells. Biochem Biophys Res Commun. 2005;337(2):498-504. doi:10.1016/j.bbrc.2005.09.073
42. Inoue K, Slaton JW, Eve BY, et al. Interleukin 8 Expression Regulates Tumorigenicity and Metastases in Androgen-independent Prostate Cancer Interleukin 8 Expression Regulates Tumorigenicity and Metastases in Androgen-independent Prostate Cancer 1. 2000;6(May):2104-2119.
43. Cai G, Wu D, Wang Z, et al. Collapsin response mediator protein-1 (CRMP1) acts as an invasion and metastasis suppressor of prostate cancer via its suppression of epithelial–mesenchymal transition and remodeling of actin cytoskeleton organization. Oncogene. 2017;36(4):546-558. doi:10.1038/onc.2016.227
44. Wu X, Gong S, Roy-burman P, Lee P, Culig Z. Current mouse and cell models in prostate cancer research. 2013;(Table 1). doi:10.1530/ERC-12-0285
45. Gupta GP, Massagué J. Cancer Metastasis: Building a Framework. Cell. 2006;127(4):679-695. doi:10.1016/j.cell.2006.11.001
46. Steeg PS. Tumor metastasis : mechanistic insights and clinical challenges. 2006;12(8):895-904. doi:10.1038/nm1469
47. Bos PD, Zhang XH-F, Nadal C, et al. Genes that mediate breast cancer metastasis to the brain. Nature. 2009;459(7249):1005-1009. doi:10.1038/nature08021
48. Mori K, Le Goff B, Charrier C, Battaglia S, Heymann D, Rédini F. DU145 human prostate cancer cells express functional receptor activator of NFκB: New insights in the prostate cancer bone metastasis process. Bone. 2007;40(4):981-990. doi:10.1016/j.bone.2006.11.006
49. Bone H, Nemeth JA, Harb JF, et al. Severe Combined Immunodeficient-hu Model of Human Prostate Cancer Metastasis. 1999;(313):1987-1993.
50. Fisher JL, Schmitt JF, Howard ML, Mackie PS, Choong PFM, Risbridger GP. An in vivo model of prostate carcinoma growth and invasion in bone. Cell Tissue Res. 2002;307(3):337-345. doi:10.1007/s00441-001-0503-x
51. Poste G, Doll J, Hart IR, Fidler IJ. Tissue-invasive Properties. 1980;40(May).
52. Yoneda T, Williams PJ, Hiraga T, Niewolna M. A Bone-Seeking Clone Exhibits Different Biological Properties from the MDA-MB-231 Parental Human Breast Cancer Cells and a Brain-Seeking Clone In Vivo and In Vitro.
53. Fidler IJ. Hypothesis Revisited. 2003;3(June):1-6.
54. Leong HS, Robertson AE, Stoletov K, et al. Invadopodia Are Required for Cancer Cell Extravasation and Are a Therapeutic Target for Metastasis. Cell Rep. 2014;8(5):1558-1570. doi:10.1016/j.celrep.2014.07.050
55. Wirtz D, Konstantopoulos K, Searson PC. The physics of cancer: the role of physical interactions and mechanical forces in metastasis. Nat Rev Cancer. 2011;11(7):512-522. doi:10.1038/nrc3080
56. Charras G, Sahai E. Physical influences of the extracellular environment on cell migration. Nat Rev Mol Cell Biol. 2014;15(12):813-824. doi:10.1038/nrm3897
57. Gligorijevic B, Wyckoff J, Yamaguchi H, Wang Y, Roussos ET, Condeelis J. N-WASP-mediated invadopodium formation is involved in intravasation and lung metastasis of mammary tumors. J Cell Sci. 2012;125(3):724-734. doi:10.1242/jcs.092726
58. Oser M, Dovas A, Cox D, Condeelis J. European Journal of Cell Biology Nck1 and Grb2 localization patterns can distinguish invadopodia from podosomes. Eur J Cell Biol. 2011;90(2-3):181-188. doi:10.1016/j.ejcb.2010.08.006
59. Linder S. Invadosomes at a glance. J Cell Sci. 2009;122(17):3009-3013. doi:10.1242/jcs.032631
60. Haffner MC, Esopi DM, Chaux A, et al. AIM1 is an actin-binding protein that suppresses cell migration and micrometastatic dissemination. Nat Commun. 2017;8(1):142. doi:10.1038/s41467-017-00084-8